Synthesis of PtSn/Carbon Nanocomposites Using *trans*-$PtCl(PEt_3)_2(SnCl_3)$ as the Source of Metal

Deborah L. Boxall,† Edward A. Kenik,‡ and C. M. Lukehart*,†

Department of Chemistry, Vanderbilt University, Nashville, Tennessee 37235, and Metals and Ceramics Division, Oak Ridge National Laboratory, Oak Ridge, Tennessee 37831

Received October 10, 2001. Revised Manuscript Received January 25, 2002

Five Pt−Sn/Vulcan carbon nanocomposites containing metal nanoclusters highly dispersed on a carbon powder support have been prepared using *trans*-$PtCl(PEt_3)_2(SnCl_3)$ as the source of metal. Thermal gravimetric analysis of the decomposition of this complex in air reveals a single-step loss of all nonmetallic elements centered at 243 °C. X-ray diffraction (XRD) analysis confirms formation of PtSn (niggliite) nanocrystals as the only crystalline phase present in the nanocomposite products, excluding trace contamination by Pt metal in one sample. Pt/Sn atomic ratios determined from on-particle high-resolution energy-dispersive spectroscopy (HR-EDS) measurements are consistent with the formation of PtSn nanocrystals and provide no evidence for the formation of phase-separated compositions. Metal nanoclusters are formed using single or multiple depositions of precursor with average sizes of 7−26 nm even at metal loadings as high as 40 wt %.

Introduction

Platinum and tin form five bimetallic intermetallic phases, Pt_3Sn, PtSn, Pt_2Sn_3, $PtSn_2$, and $PtSn_4$, of which Pt_3Sn and PtSn are congruently melting compositions. The PtSn phase is commonly known as the mineral niggliite. These intermetallic phases are distinguished by distinct crystalline structures and unique XRD patterns.

Pt−Sn composites are well-known for their catalytic activity, and chemistry occurring on Pt−Sn surfaces has been a topic of a number of recent reports.[1−7] Heterogeneous catalysts containing nanoparticulate Pt−Sn phases are commercial catalysts in hydrocarbon reforming and isobutane dehydrogenation.[8−14] Pt−Sn catalysts are usually supported on ceramic powders, such as silica or alumina, with the desired metal stoichiometry being achieved through proper mixing of separate Pt and Sn reagents. Although some of these syntheses yield a single Pt−Sn phase,[10] the formation of a mixture of Pt−Sn phases is more commonly observed.[12,13]

Pt−Sn/carbon nanocomposites have been studied for decades as anode catalysts for the electrooxidation of methanol and other small carbohydrate fuels.[15,16] These nanocomposites have been prepared by a variety of electrochemical or chemical deposition methods, and inconsistencies in catalyst performance have been attributed primarily to the lack of compositional purity of catalyst particles. Synthetic strategies for preparing Pt−Sn/C nanocomposites of uniform composition and structure are clearly needed, particularly for electrocatalytic applications.

As part of an ongoing investigation into the preparation of metal alloy/carbon nanocomposites exhibiting high performance as methanol electrooxidation catalysts, we have reported Pt−Ru/carbon nanocomposites having electrocatalytic performances comparable or even superior to that of unsupported Pt−Ru colloid, which serves as a practical standard of performance.[17−22]

* To whom correspondence should be addressed.
† Vanderbilt University.
‡ Oak Ridge National Laboratory.

(1) Gertosio, V.; Santini, C. C.; Taoufik, M.; Bayard, F.; Basset, J. M.; Buendia, J.; Vivat, M. *J. Catal.* **2001**, *199*, 1.
(2) Rodriguez, J. A.; Jirsak, T.; Chaturvedi, S.; Hrbek, J. *J. Am. Chem. Soc.* **1998**, *120*, 11149.
(3) Tsai, Y. L.; Koel, B. E. *Langmuir* **1998**, *14*, 1200.
(4) Humblot, F.; Didillon, D.; Lepeltier, F.; Candy, J. P.; Corker, J.; Clause, O.; Bayard, F.; Basset, J. M. *J. Am. Chem. Soc.* **1998**, *120*, 137.
(5) Szanyi, J.; Paffett, M. T. *J. Am. Chem. Soc.* **1995**, *117*, 1034.
(6) Peck, J. W.; Koel, B. E. *J. Am. Chem. Soc.* **1996**, *118*, 2708.
(7) Xu, C.; Peck, J. W.; Koel, B. E. *J. Am. Chem. Soc.* **1993**, *115*, 751.
(8) Casella, M. L.; Siri, G. J.; Santori, G. F.; Ferretti, O. A. *Langmuir* **2000**, *16*, 5639.
(9) Arana, J.; Ramirez de la Piscina, P.; Llorca, J.; Sales, J.; Homs, N. *Chem. Mater.* **1998**, *10*, 1333.
(10) Llorca, J.; Ramirez de la Piscina, P.; Fierro, J. L. G.; Sales, J.; Homs, N. *J. Catal.* **1995**, *156*, 139.
(11) Yarusov, I. B.; Zatolokina, E. V.; Shitova, N. V.; Belyi, A. S.; Ostrovski, N. M. *Catal. Today* **1992**, *13*, 655.
(12) Srinivasan, R.; Rice, L. A.; Davis, B. H. *J. Catal.* **1991**, *129*, 257.
(13) Srinivasan, R.; De Angelis, R. J.; Davis, B. H. *J. Catal.* **1987**, *106*, 449.
(14) Burch, R.; Garla, L. C. *J. Catal.* **1981**, *71*, 360.
(15) Mukerjee, S.; McBreen, J. *J. Electrochem. Soc.* **1999**, *146*, 600 and references therein.
(16) Gonzalez, M. J.; Hable, C. T.; Wrighton, M. S. *J. Phys. Chem. B* **1998**, *102*, 9881.
(17) Boxall, D. L.; Deluga, G. A.; Kenik, E. A.; King, W. D.; Lukehart, C. M. *Chem. Mater.* **2001**, *13*, 891.
(18) Boxall, D. L.; Lukehart, C. M. *Chem. Mater.* **2001**, *13*, 891.
(19) Lukehart, C. M.; King, W. D.; Milne, S. B.; Jones, F. E., III.; Corn, J. D.; Boxall, D. L.; Kwiatkowski, K. C. U.S. Patent 6,232,264, May 15, 2001.
(20) Kwiatkowski, K. C.; Lukehart, C. M.; Murphy, O. J.; Simpson, S. F. *J. Cluster Sci.* **2000**, *11*, 449.
(21) Boxall, D. L.; Corn, J. D.; Jones, E. F., III.; King, W. D.; Lukehart, C. M. *Fuel Cell Semin. Abstr.* **1998**, 545.
(22) Lukehart, C. M.; Boxall, D. L.; Corn, J. D.; Hariharasarma, M.; King, W. D.; Kwiatkowski, K. C.; Steigerwalt, E. S.; Kenik, E. A. *ACS Fuel Chem. Div. Prepr.* **1999**, *44*, No. 4, 982.

10.1021/cm010952j CCC: $22.00
Published on Web 03/08/2002

These nanocomposites were prepared using a bimetallic precursor as the source of Pt and Ru and through careful control of thermal treatments. We are extending this method to other binary metal alloy/carbon compositions with the aim of discovering electrooxidation catalysts having enhanced performance over those prepared by more conventional methods.

We now report the synthesis and characterization of a PtSn/Vulcan carbon powder nanocomposite using the bimetallic complex *trans*-$PtCl(PEt_3)_2(SnCl_3)$ as the source of metal. Reactive, thermal treatment of *trans*-$PtCl(PEt_3)_2(SnCl_3)$/Vulcan carbon composites at relatively mild temperatures gives PtSn/carbon nanocomposites containing nanocrystals of PtSn (niggliite) widely dispersed on the carbon support. Phase separation of the metals to form other Pt−Sn compositions can be avoided. Related Pt−Sn bimetallic complexes have been used as precursors in the formation of a PtSn/silica xerogel nanocomposite[23,24] and PtSn catalysts supported on silica or γ-alumina.[25]

Experimental Section

General Methods. *cis*-Dichloro-bis(triethylphosphine)platinum(II) was purchased from Aldrich Chemical Co. Anhydrous tin(II) chloride (98%) was purchased from Alpha. Dichloromethane (Fisher Chemical Company) was distilled over calcium hydride and molecular sieves (Aldrich, 4-Å pore size) prior to use. Vulcan carbon XC-72R was purchased from Cabot Corporation and was used as received.

Thermogravimetric analysis (TGA) of a sample of Vulcan carbon with adsorbed precursor was performed using a TA Instruments Hi-Res TGA 2950 apparatus under air at a 15 °C/min ramp rate to mimic the heating rate that can be obtained in tube furnace preparations. Surface-area measurements and adsorption/desorption isotherms were obtained using a Quantachrome Nova 1000 high-speed surface-area analyzer.

Particle-size distributions for nanocomposite materials were obtained using a Philips CM20T transmission electron microscope (TEM) operating at 200 kV in the bright-field mode. Single-particle high-spatial-resolution energy-dispersive spectroscopy (HR-EDS) was used to examine variations in particle composition using a Philips CM200FEG 200kV TEM equipped with an Oxford light element EDS detector and an EMiSPEC Vision data acquisition system in the SHaRE Collaboration Research Center in the Metals and Ceramics Division of Oak Ridge National Laboratory. The HR-EDS data were collected using a tilt angle of 15°, a detector elevation angle of 20°, an acceleration voltage of 200 kV, a collection time of 20 s, and a 1.4-nm-diameter probe in the stopped-scan mode. Integrated intensities from the Pt $L_{\alpha 1}$ and Sn $L_{\alpha 1}$ lines were used for quantification, as they were not overlapped by any other X-ray emissions. The X-ray emission cross sections appropriate for the instrumental geometry and the spurious contributions from the Vulcan carbon support were obtained by measuring Pt and Sn emission intensities for 100 s from several 1 μm^2 areas of a sample having a known bulk chemical composition.

XRD scans were obtained using a Scintag X_1 θ/θ automated powder diffractometer with a Cu target and a Peltier-cooled solid-state detector. Samples were prepared by covering a 25 mm × 10 mm area of a zero-background Si(510) substrate with a uniform layer of nanocomposite. Each nanocomposite was scanned from 20° to 140° in 2θ using a step-scan mode at a scan rate of 0.02°/s and a 1-s collection time per step. The background-corrected XRD scan was used to confirm the presence of the PtSn niggliite phase as well as the absence of any other crystalline phases.

Bulk chemical microanalyses were performed by Galbraith Laboratories, Knoxville, TN. Samples for metal analysis were subjected to a H_2SO_4/HCl/HNO_3 acid digestion prior to determination of Pt and Sn content by inductively coupled plasma optical emission spectroscopy (ICP-OES). Carbon and hydrogen analyses were performed by combustion under an O_2 atmosphere at 1000 °C using a Leco Corp. combustion analyzer.

Preparation of *trans*-[$PtCl(PEt_3)_2(SnCl_3)$], 1. The PtSn molecular precursor, **1**, was prepared using the method reported by Pregosin and Sze.[26] Specifically, 190 mg (1.0 mmol) of anhydrous $SnCl_2$ was added to a solution containing 52 mg (0.10 mmol) of *cis*-$PtCl_2(PEt_3)_2$ dissolved in 25 mL of distilled CH_2Cl_2. The suspension was stirred for 1 h under N_2 and then was filtered through a layer of Celite 545 supported on a medium frit to afford a bright yellow solution. Precursor **1** was isolated as a light yellow powder upon removal of the solvent at reduced pressure. Yield, 64 mg (88%); mp, 84−88 °C (literature value = 92 °C).[26] Compound purity was verified by ^{1}H NMR spectral data.

Preparation of PtSn/C Nanocomposites 2a−2e. The air and N_2 gases used during thermal treatments were passed over a 30-cm column of Drierite (anhydrous $CaSO_4$) at a rate of 200 mL/min. Getter gas (10% H_2/90% N_2 mix; A.L. Gas, Nashville, TN) was used as received at a flow rate of 200 mL/min. Thermal treatments were performed on samples placed into an alumina combustion boat (Fisher, Corning 60035) and inserted into a Lindberg programmable tube furnace. Specific data on sample preparation and characterization are provided in Table 1. Nanocomposites were prepared using either a single deposition of precursor (method A) or multideposition of precursor (method B) as described below.

Method A. To a specified mass of precursor **1** dissolved in 20 mL of CH_2Cl_2 was added the appropriate mass of Vulcan carbon powder to give the desired total metal loading. The resulting suspension was stirred at room temperature for 3 h. After 1 h of stirring, the yellow color of precursor **1** could not be seen. Residual solvent was removed at reduced pressure to ensure complete deposition of precursor onto the carbon support. The resulting precursor/carbon composite was first heated to 250 °C under air at a rate of 15 °C/min to effect oxidative decomposition of the precursor. The furnace was then purged with N_2 for 15 min before being switched to getter gas (10% H_2/90% N_2). While under a getter gas atmosphere, the temperature of reaction was increased to 650 °C at a rate of 15 °C/min. The atmosphere was then switched back to N_2, and the temperature was held at 650 °C for 1 h to improve the crystallinity of the formed nanocrystals. The furnace was allowed to cool to ambient conditions under a N_2 atmosphere over a period of ca. 3 h, and the PtSn/carbon nanocomposite was isolated as a dry black powder.

Method B. Three equal depositions of precursor were utilized in this method. The first portion of precursor was deposited onto the carbon powder support from CH_2Cl_2 solution as described above in method A. After removal of the solvent at reduced pressure, the precursor/carbon composite was transferred to an alumina combustion boat and inserted into the tube furnace. The composite was first heated to 250 °C under air at a rate of 15 °C/min to effect oxidative decomposition of the precursor. The furnace was then purged with N_2 for 15 min before being switched to a getter gas atmosphere and increasing the temperature of the furnace to 650 °C at a rate of 15 °C/min. The atmosphere was then switched back to N_2, and the reaction temperature was held at 650 °C for 5 min. After the composite had been cooled to ambient conditions under N_2, a second portion of precursor **1** was deposited on the carbon support by stirring a suspension containing the once-treated carbon in a solution of 50 mL of CH_2Cl_2 and the appropriate amount of precursor **1**. The resulting composite

(23) Carpenter, J. P.; Lukehart, C. M.; Stock, S. R. *J. Organomet. Chem.* **2000**, *596*, 252.

(24) Carpenter, J. P.; Lukehart, C. M.; Milne, S. B.; Stock, S. R.; Wittig, J. E.; Jones, B. D.; Glosser, R.; Henderson, D. O.; Mu, R.; Shull, R. D.; Zhu, J. G.; Rek, Z. U. *Int. SAMPE Technol. Conf.* **1995**, *27*, 549.

(25) Llorca, J.; de la Piscina, P. R.; Fierro, J. L. G.; Sales, J.; Homs, N. *J. Mol. Catal. A: Chem.* **1997**, *118*, 101.

(26) Pregosin, P. S.; Sze, S. N. *Helv. Chim. Acta* **1978**, *61*, 1848.

Table 1. Preparation and Characterization Data for PtSn/Carbon Nanocomposites 2A−2E

sample	2a	2b	2c	2d	2e
precursor **1**, mg	50	62	117	265	556
Vulcan carbon, mg	50	40	53	302	251
thermal treatment[a]	method A	method A	method A	method B	method B
C, wt %	66.04	66.21	49.63	68.19	55.34
H, wt %	<0.5	<0.5	<0.5	<0.5	<0.5
Pt, wt %	19.98	13.85	24.29	11.61	18.53
Sn, wt %	6.79	8.53	15.21	9.03	7.86
P, wt %	0.45	–	–	–	0.48
total metal, wt %	26.8	22.4	39.5	20.6	26.4
Pt/Sn atomic ratio	1.79	0.99	0.97	0.78	1.43
avg diam, TEM, nm (esd)[b]	20 (9)	12 (1)	26 (12)	7 (2)	10 (5)
avg diam, XRD, nm (esd)[b]	27 (3)	17 (3)	28 (5)	13 (4)	13 (2)
lattice constant a_0, Å (esd)[b,c]	4.120 (8)	4.10 (1)	4.09 (1)	4.09 (1)	4.119 (6)
lattice constant c_0, Å[d]	5.456	5.432	5.429	5.413	5.450
BET surface area, m^2/g	139	117	115	143	108

[a] Method A: Single deposition of precursor; 25 → 250 °C in air; 250 → 650 °C in getter gas; 650 °C, getter gas, 1 h. Method B: Three equal depositions of precursor; 25 → 250 °C in air; 250 → 650 °C in getter gas; 650 °C, getter gas, 5 min; final anneal at 650 °C under N_2 for 1 h. [b] esd = estimated standard deviation in last significant digit. [c] Uniquely determined independently from the (100), (110), (210), and (300) peak positions. [d] Uniquely determined from the (004) peak position.

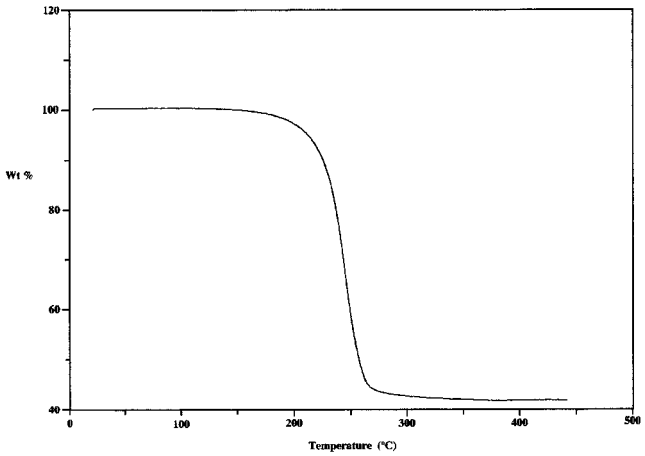

Figure 1. TGA analysis of the thermal decomposition of *trans*-$PtCl(PEt_3)_2(SnCl_3)$, **1**, in air showing single-step elimination of nonmetal mass.

was thermally treated as before, with only a 5-min anneal at 650 °C. The third and final portion of precursor **1** was deposited on the carbon support by stirring a suspension containing the twice-treated carbon in a solution of 50 mL of CH_2Cl_2 containing the third portion of precursor **1**. The resulting composite was heated under air to 250 °C at 15 °C/min, purged with N_2 for 15 min, and then heated to 650 °C under a getter gas atmosphere at a ramp rate of 15 °C/min. After being switched to a N_2 atmosphere, the nanocomposite was annealed at a temperature of 650 °C for 1 h. The nanocomposite was allowed to cool to ambient conditions under a N_2 atmosphere, and the PtSn/carbon nanocomposite was isolated as a dry black powder.

Results and Discussion

As shown in Figure 1, a TGA trace of the thermal decomposition of *trans*-$PtCl(PEt_3)_2(SnCl_3)$, **1**, in air from ambient temperature to >400 °C reveals a remarkable single-step mass loss centered at 243 °C. This mass loss corresponds to complete loss of the PEt_3 ligands and Cl, giving a residual mass equal to the total metal content of precursor **1** (45 wt %).

Reactive degradation of complex **1** deposited on Vulcan carbon powder at arbitrary loading under appropriate conditions leads to the formation of PtSn/carbon nanocomposites **2a**−**2e**, as depicted in eq 1. Specific data for the preparation and characterization of these five PtSn/carbon nanocomposites are provided in Table 1.

Each nanocomposite is prepared from a precursor **1**/carbon composite using mild heating in air (25−250 °C) to degrade the precursor to its metallic content followed by thermal annealing at 250−650 °C under slightly reducing conditions (10:90 H_2/N_2) to favor formation of highly crystalline nanoparticles. The total metal loading of the resulting PtSn/carbon nanocomposites range from 21 to 40 wt %. Nanocomposites were prepared using either single (**2a**−**2c**) or multiple (**2d** and **2e**) depositions of precursor **1** to determine any effect of the precursor deposition protocol on the average size or size distribution of the resulting nanoparticles. Pt/Sn atomic ratios calculated for nanocomposites **2a**−**2e** from commercial bulk chemical microanalysis data range from 0.78 to 1.79, with an average Pt/Sn stoichiometry of 1.2, indicating either considerable variation in bulk Pt−Sn content or difficulties in obtaining reproducible metal microanalysis. Given the preponderance of evidence supporting the formation of PtSn niggliite particles in these nanocomposites with no evidence of significant phase separation, as discussed below, we speculate that reproducible bulk metal analyses for these carbon-supported nanocomposites might be problematic.

The specific surface areas of nanocomposites **2a**−**2e** shown in Table 1 decrease in value with increasing metal content. When corrected for the mass of metal present within each sample, these values are within the experimental error of the surface area of Vulcan carbon powder (240 m^2/g). The mesoporous structure of the carbon support does not appear to be significantly altered during nanocomposite synthesis.

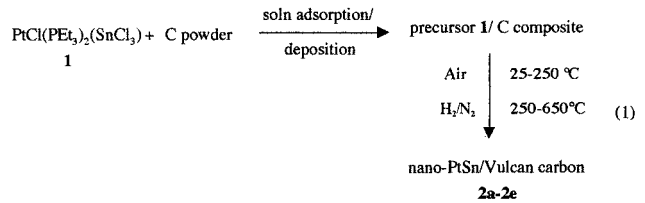

Bright-field TEM images of nanocomposites **2a**−**2e** reveal metal particles of high contrast that are well dispersed on the carbon support. A representative TEM micrograph is shown in Figure 2 for nanocomposite **2a**. Metal particles having irregular spheroidal shapes as

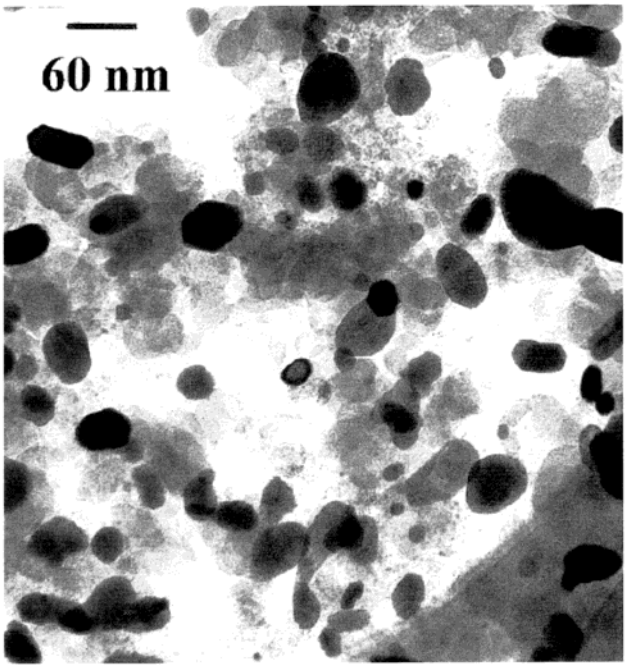

Figure 2. Representative bright-field TEM micrograph of the PtSn/carbon nanocomposite **2a**.

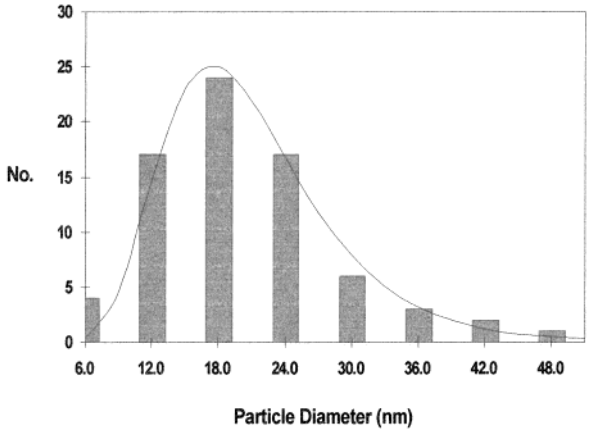

Figure 3. Histogram of metal particle diameters observed in the PtSn/carbon nanocomposite **2a**.

well as faceted hexagonal shapes are observed in this nanocomposite. Hexagonal nanocrystals of PtSn (niggliite, $P6_3/mmc$) have also been observed in PtSn/silica xerogel nanocomposites.[23,24] A significant fraction of metal nanoparticles present in nanocomposite **2c** are needle-shaped. This nanocomposite has the highest total metal content (40 wt %) and was prepared using a single deposition of precursor. A high surface density of deposited metal would favor extended particle growth from initial nucleation sites.

Histograms of metal particle diameters measured directly from TEM micrographs reveal log−normal particle size distributions, as shown in Figure 3 for nanocomposite **2a**. Both the shapes and widths of these particle size distributions are indicative of particle growth controlled by surface-diffusion mechanisms.[27] The average diameters of the metal nanoparticles in nanocomposites **2a**−**2e** range from 7 to 26 nm, with nanocomposite **2c** having the largest average metal particle size and the highest metal loading. Nanocomposites **2a** and **2b** (prepared by method A) have respective average particle sizes that are at least 50% larger than those of nanocomposites **2e** and **2d** (prepared by method B) at comparable metal loading. This observation suggests that a multistep deposition of precursor is the synthesis protocol of choice for preparing small metal particles at high metal loading.

A typical broad-area EDS spectrum is shown in Figure 4 for nanocomposite **2e**. Intense X-ray emission occurs from several lines of Pt and Sn, as expected. Copper emission from the specimen grid holding the sample is also observed. A magnified view of the EDS spectrum below 4 keV indicates no observable emission from the strongest lines of Cl or P. Emission intensity from the Pt Mα line does interfere with the detection of the low-intensity P emission, however. Although nanocomposites **2a** and **2e** contain <0.5 wt % phosphorus by bulk microanalysis, there is no clear evidence for the retention of either Cl or P in these nanocomposites at the EDS detection limit. EDS data support the complete degradation of precursor **1** to Pt−Sn metal, as observed by TGA.

XRD scans of nanocomposites **2a**−**2e** display the pattern of peaks expected for PtSn (niggliite), as shown in Figure 5 for nanocomposite **2e**. Evidence for the formation of PtP_2 impurity or other Pt−Sn intermetallic phases is absent. Although nanocomposites **2a** and **2e** apparently contain excess Pt metal by bulk microanalysis, Pt cannot be identified by XRD in these samples. Only a trace amount of Pt metal is evident in the XRD pattern of nanocomposite **2c**.

XRD peak positions and relative intensities match well with the XRD line pattern known for PtSn (niggliite); see Figure 5. The positions of the (100), (110), (210), and (300) diffraction peaks were used to calculate the a_0 lattice constants listed in Table 1 assuming a hexagonal cell. The positions of the (004) diffraction peaks were used to calculate the corresponding c_0 lattice constants. These calculated lattice constants are within 2 standard deviations of those known for PtSn (niggliite; a_0 = 4.100 Å, c_0 = 4.432 Å), indicating a lack of significant lattice strain within the PtSn nanocrystals. PtSn nanocrystals in nanocomposites **2a**−**2e** have average domain sizes of 13−27 nm, as calculated from XRD peak width measurements using Scherrer's equation.[28] The close correspondence observed between PtSn particle sizes measured directly by TEM and domain sizes determined from XRD data indicates both the absence of a significant fraction of atypically large metal particles in these nanocomposites and PtSn nanocrystals having single-domain crystallinity.

To further investigate the compositional integrity of PtSn nanocrystals prepared using this synthetic strategy, the Pt/Sn atomic ratios of 49 randomly chosen nanocrystals within nanocomposite **2e** were measured experimentally by HR-EDS. The integrated intensities of the Pt $L_{\alpha 1}$ and Sn $L_{\alpha 1}$ emissions from *individual* alloy nanoclusters were collected using a field-emission gun

(27) Granqvist, C. G.; Buhrman, R. A. *J. Catal.* **1976**, *42*, 477.

(28) Prior to peak width measurements, diffraction peaks were corrected for background scattering and were stripped of the $K\alpha_2$ portion of the diffraction intensity. See: Klug, H. P.; Alexander, L. E. *X-ray Diffraction Procedures for Polycrystalline and Amorphous Materials*, 2nd ed.; Wiley: New York, 1974.

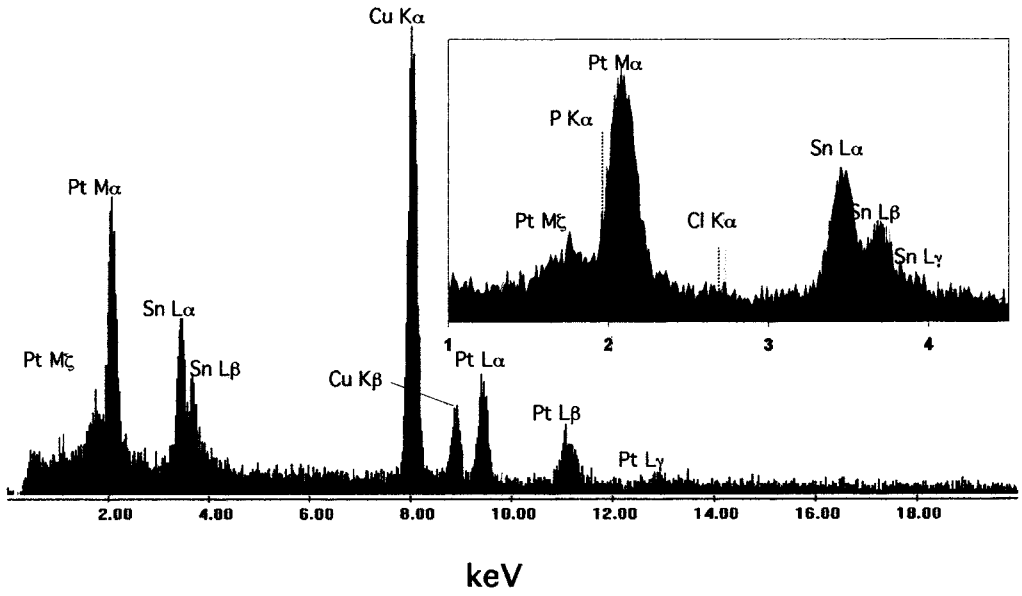

Figure 4. Broad-area EDS spectra of the PtSn/carbon nanocomposite **2e**. X-ray emission from the Cu grid sample holder is also evident. Inset shows lower-energy emission at an expanded scale.

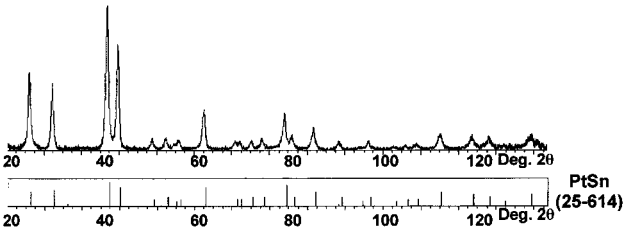

Figure 5. Powder XRD scan of nanocomposite **2e** along with the standard XRD line pattern for PtSn (niggliite), PDF card 25-614.

with a spot size of 1.4 nm. A plot of Pt emission intensity vs Sn emission intensity for all of the particles examined is linear, as expected for particles containing nearly equal numbers of Pt and Sn atoms where Pt and Sn emission cross sections differ by a constant factor. Experimental intensities were converted into Pt/Sn atomic ratios by using a standard sample as a reference.

A plot of Pt/Sn atomic ratio versus nanocluster diameter for the 49 metal nanocrystals chosen within nanocomposite **2e** is shown in Figure 6. Error bars for the Pt/Sn atomic ratios are calculated from error propagation and are based principally on the EDS counting statistics. Low emission intensities from the smallest particles afford greater error in particle composition. The particle-size distribution of those metal nanoclusters randomly chosen for on-particle HR-EDS measurements is essentially identical to that determined from TEM micrographs (see Figure 3).

As to compositional variation on the nanocluster scale, only statistical arguments can be made. A standard deviation calculated for the mean Pt/Sn atomic ratio, weighted for the experimental uncertainty associated with each on-particle measurement, is ±0.18. This error is due principally to experimental uncertainties associated with the HR-EDS counting statistics but also includes particle-to-particle variations in metal stoichiometry. However, this experiment does demonstrate that gross phase separation of the two metals does not occur with high frequency during the formation of these nanocomposites. HR-EDS measurements also indicate

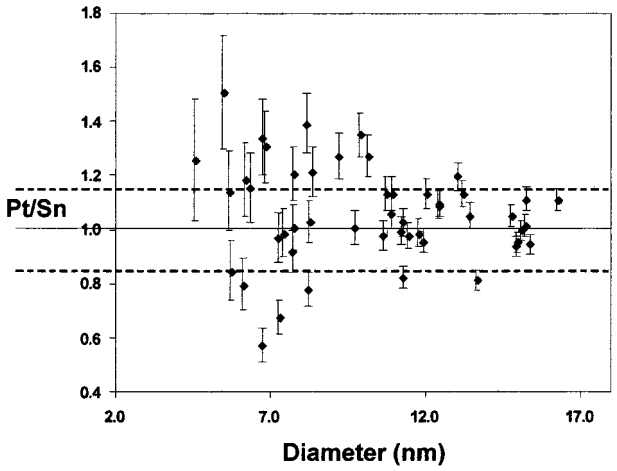

Figure 6. Plot of on-particle Pt/Sn stoichiometries for 49 metal particles of nanocomposite **2e** determined by EDS as a function of nanoparticle size (dashed lines show 1σ limits).

the absence of detectable amounts of Pt or Sn in regions of the carbon support not containing nanoparticles. This observation suggests that metal content is localized primarily within observable metal nanoparticles and that excess metal content measured by commercial bulk chemical microanalysis might be due to experimental uncertainty. The average Pt/Sn stoichiometry of the 47 nanoclusters examined within nanocomposite **2e** is 1.06(18). This composition is within one standard deviation of the average Pt/Sn stoichiometry of 1.2 determined by bulk chemical microanalysis and within one standard deviation of the 1:1 Pt/Sn stoichiometry of precursor **1**.

Conclusions

(1) The complex *trans*-$PtCl(PEt_3)_2(SnCl_3)$ undergoes remarkable oxidative degradation near 250 °C with loss of its nonmetallic elements and serves as an excellent single-source precursor for Pt and Sn.

(2) Reactive degradation of $PtCl(PEt_3)_2(SnCl_3)$/carbon composites affords PtSn/carbon nanocomposites con-

taining metal nanocrystals widely dispersed on the carbon support. Under appropriate conditions, the only crystalline phase observed in these nanocomposites is PtSn (niggliite). This synthesis procedure thus compliments methods used to prepare Pt_3Sn/carbon nanocomposites as fuel cell anode catalysts.[15] By using a multistep protocol for precursor deposition, PtSn nanocrystals of 10-nm average diameter can be prepared at a total metal loading of 26 wt %. PtSn nanocrystals of smaller average particle size might be formed by using lower metal loadings or rapid thermal processing.[18]

(3) On-particle EDS measurements confirm localization of metal within the observed nanocrystals and metal nanoparticle compositions near a 1:1 Pt/Sn stoichiometry. More precise methods for determining the stoichiometry of individual nanoparticles are needed.

Acknowledgment. Research support provided by the U.S. Army Research Office under Grants DAAH04-95-1-0146, DAAH04-96-1-0179, DAAH04-96-1-0302, and DAAG55-98-1-0362 is gratefully acknowledged by C.M.L. On-particle EDS and HR-TEM measurements performed at the Oak Ridge National Laboratory SHaRE Collaborative Research Center was sponsored by the Division of Materials Sciences and Engineering, U.S. Department of Energy, under Contract DE-AC05-00OR22725 with UT-Battelle, LLC, and through the SHaRE Program under Contract DE-AC05-76OR00033 with Oak Ridge Associated Universities. This article was authored by a contractor of the U.S. Government under Contract DE-AC05-00OR22725. Accordingly, the U.S. Government retains a nonexclusive, royalty-free license to publish or reproduce the published form of this contribution or allow others to do so for U.S. Government purposes.

CM010952J